

Cite this: *Chem. Sci.*, 2025, 16, 8338

All publication charges for this article have been paid for by the Royal Society of Chemistry

## Double helicene possessing B–N dative bonds built on 1,4-dihydropyrrolo[3,2-*b*]pyrrole core†

Wojciech D. Petrykowski,<sup>ab</sup> Nicolas Vanthuynne,<sup>c</sup> Carmelo Naim,<sup>d</sup> Francesco Bertocchi,<sup>e</sup> Yevgen M. Poronik,<sup>a</sup> Arkadiusz Ciesielski,<sup>b</sup> Michał K. Cyrański,<sup>ab</sup> Francesca Terenziani,<sup>be</sup> Denis Jacquemin<sup>df</sup> and Daniel T. Gryko<sup>ab</sup>

Just four steps are required to transform 2-nitrobenzaldehyde into centrosymmetric, quadrupolar N,B-doped nanographenes possessing two nitrogen–boron dative bonds. A convergent fragment coupling strategy allowed rapid access to key intermediates bearing the 1,4-dihydropyrrolo[3,2-*b*]pyrrole core. 2,6-Di-*tert*-butylpyridine turned out to be the best base for the formation of B←N bonds. This synthetic strategy can be extended to encompass double helicenes possessing two [7]helicene units bearing four five-membered rings. The size of the peripheral arm influences the reaction output: in the case of replacing benzene with dibenzothiophene, the yield decreases from 75% to 16%. Interestingly only two enantiomers and not *meso* form are formed in the latter case. The obtained double helicene containing 14 fused rings, exhibits green emission characterized by reasonable fluorescence quantum yield reaching 0.38. This dye has average circularly polarized luminescence brightness ( $B_{CPL}$ ) of about  $15 \text{ M}^{-1} \text{ cm}^{-1}$ . The analysis of the electronic structure of the dyes with quantum chemical methods reveals highly-delocalized excited states with the core of the dye acting as an electron-donating moiety.

Received 21st January 2025  
Accepted 2nd April 2025

DOI: 10.1039/d5sc00540j

rsc.li/chemical-science

## Introduction

The incorporation of boron–nitrogen bonds into the structure of polycyclic aromatic hydrocarbons (PAHs) offers polarization of  $\pi$ -systems, which leads to the modulation of their photo-physical properties. The extraordinary advances in the chemistry of azaborines have been fueled by the isosteric character of the N–B bond *versus* the C=C bond.<sup>1–10</sup> In contrast, the approach to aromatic architectures with B←N dative bonds has a much shorter history which started from a key paper by Yamaguchi in 2006.<sup>11</sup> The presence of four-coordinated boron

atoms in such dyes represents an entirely new handle for tuning the optoelectronic properties.<sup>12,13</sup> During the last decade, Jäkle and co-workers described several polycyclic structures possessing two B←N bonds *e.g.* dye **1** (Fig. 1).<sup>14–17</sup> Extensive efforts have been devoted to advancing this chemistry by Pischel and Nakamura in 2020, who reported a bis-boronated green light-emitter **2**, which possessed a nearly quantitative fluorescence quantum yield ( $\Phi_f$ ) (Fig. 1).<sup>18,19</sup> Similarly, in 2021, we reported a polarized B←N-containing chromophore **3** with an electron-donating 1,4-dihydropyrrolo[3,2-*b*]pyrrole system incorporated into its central part to obtain derivatives that show efficient green and red light emission.<sup>20</sup> However, the chemical diversity of these structures cannot cover the fact that until recently the vast majority of functional dyes possessing B←N bonds had a planar  $\pi$ -system.

Within the quest of discovering organic chromophores possessing strong circularly polarized luminescence (CPL), attention has been focused on helicenes – inherently chiral polycyclic aromatic compounds composed of rings condensed in the *ortho* position in a way that they twist into a helix shape.<sup>21–24</sup> The main arguments driving research on helicenes are possible applications of CPL which include OLEDs,<sup>25</sup> fluorescence microscopy,<sup>26</sup> *etc.*<sup>22</sup> It is obvious that materials other than archetypal benzene-only helicenes may offer greater chemical variability and more appreciable chiroptical properties.<sup>27–39</sup> Among many heterocyclic helicenes, dyes possessing an azaborine moiety were reported in a few works.<sup>40–42</sup>

<sup>a</sup>Institute of Organic Chemistry, Polish Academy of Sciences, Kasprzaka 44-52, 01-224 Warsaw, Poland. E-mail: dtgryko@icho.edu.pl

<sup>b</sup>Faculty of Chemistry, University of Warsaw, Żwirki i Wigury 101, 02-089 Warsaw, Poland. E-mail: mkc@chem.uw.edu.pl

<sup>c</sup>Aix Marseille Univ, CNRS, Centrale Med, FSCM, Marseille, France

<sup>d</sup>Nantes Université, CNRS, CEISAM, UMR6230, F-44000, Nantes, France. E-mail: Denis.Jacquemin@univ-nantes.fr

<sup>e</sup>Department of Chemistry, Life Sciences and Environmental Sustainability, University of Parma, 43124 Parma, Italy. E-mail: francesca.terenziani@unipr.it

<sup>f</sup>Institut Universitaire de France (IUF), F-75005, Paris, France

† Electronic supplementary information (ESI) available: Detailed synthetic protocols, characterization data; <sup>1</sup>H, <sup>13</sup>C{<sup>1</sup>H} NMR and HRMS spectra, computational details and analyses, photophysical measurement results, CD and CPL spectra, chiral HPLC separation data, optical rotation values, crystal structures and additional figures as cited in the main text. CCDC 2415573 and 2430266. For ESI and crystallographic data in CIF or other electronic format see DOI: <https://doi.org/10.1039/d5sc00540j>



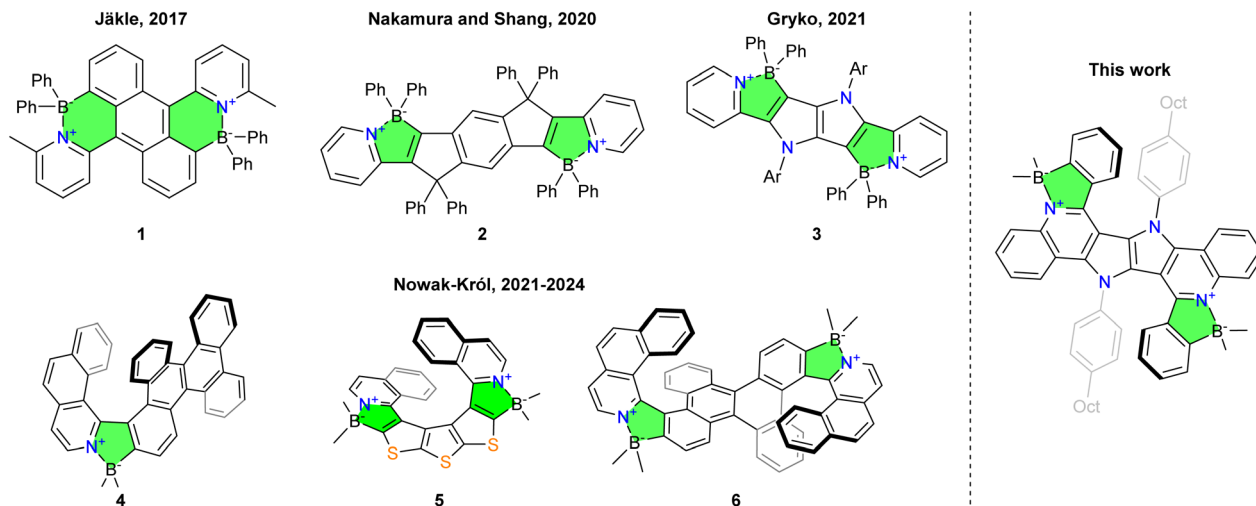


Fig. 1 Chemical structures of selected examples of dyes bearing B←N dative bonds bridging aromatic systems.

Intriguingly, as reported predominantly by Nowak-Król and co-workers, helicenes bearing B←N bond(s) possess appreciable optoelectronic properties.  $\pi$ -Expanded helicene **4** has a relatively large  $\Phi_f$  of 0.31 and  $|g_{lum}|$  of  $2.2 \times 10^{-3}$  with  $\lambda_{em}$  at 510 nm.<sup>43–45</sup> Other examples include unusual helicene **5** containing three thiophene rings fused together,<sup>46</sup> and the first double helicenes encompassing B←N bonds (e.g. **6**),<sup>47</sup> possessing bright green fluorescence and reasonable  $|g_{lum}|$  values (Fig. 1). Clearly, a better understanding of the relationship between the structure of hetero-helicenes and their chiroptical properties requires explaining how the position and the type of heteroatoms affects electronic and magnetic dipole moments. This begs the question if these parameters could be modulated by incorporating multiple B←N bonds in a double helical architecture. To tackle these challenges, we target double helicenes possessing multiple B←N dative bonds at the periphery and another heterocyclic scaffold which exhibits quadrupolar symmetry.

## Design and synthesis

In principle there are a few heterocyclic scaffolds suitable to serve as a central core in the construction of double helicenes. We have chosen 1,4-dihydropyrrolo[3,2-*b*]pyrrole (DHPP)<sup>48,49</sup> as the central core because of the following combination of properties: (1) centrosymmetric, quadrupolar skeleton with near- $C_{2h}$  symmetry; (2) strong emission intensity, which remains almost constant regardless of structural modifications; (3) straightforward synthesis leading to the formation of a densely substituted scaffold which is amenable to facile functionalization.<sup>50</sup>

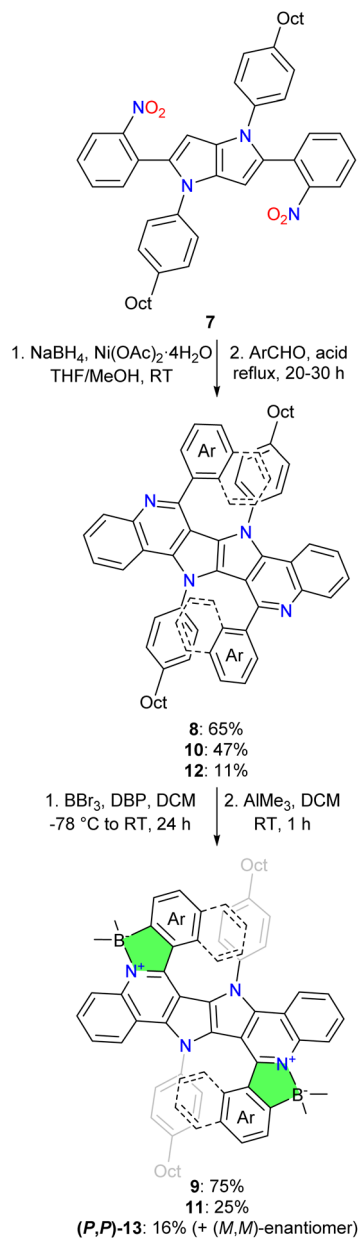
Critically the incorporation of B←N dative bonds requires the presence of a pyridine moiety within the structure. In departure from reported pathways, we conceived a convergent fragment coupling strategy starting from a multicomponent reaction leading to the DHPP core, followed by closing two pyridine rings *via* a double Pictet–Spengler reaction allowing

the installation of diverse aromatic scaffolds in the late stage. Thus, our synthetic design relies on the previously disclosed synthesis of ladder-type  $\pi$ -expanded DHPPs possessing quinoline units to build a basic centrosymmetric skeleton.<sup>51</sup> In the final step, the obtained intermediates are subjected to the reaction with boron tribromide in the presence of a base (usually DIPEA) and then the bromine atoms are replaced with methyl groups upon treatment with trimethylaluminum, as established by Murakami.<sup>52</sup>

At the outset we have chosen dye **8**, possessing simple phenyls at positions 9 and 13, as a model system, anticipating that the significant steric hindrance in the envisioned dyes would probably require optimization of the standard reaction conditions. Substrate **8** is easily accessible by the reduction/Pictet–Spengler sequence of DHPP **7** with benzaldehyde.<sup>51</sup> As for the borylation reaction, standard conditions described by Murakami<sup>52</sup> and optimized by Ingleson<sup>53</sup> give extremely low conversion of **8** and only the mono-borylated product could be isolated. We noticed that increasing the temperature significantly boosts the reaction rate, but the best results are achieved by changing the base to 2,6-di-*tert*-butylpyridine (DBP). A more challenging substrate **10**, obtained under slightly modified conditions of the aforementioned condensation, with bulkier naphthalene moieties, also undergoes electrophilic borylation to **11** with satisfactory yield thanks to the use of DBP. We underline that the syntheses of **9** and **11**, shown in Scheme 1, does not require any column chromatography, as all the products and intermediates are purified by recrystallization. Notably, although dyes **9** and **11** are formally a double [5]helicene and a double [6]helicene respectively, their racemization barrier is too low to enable separation at RT, due to the presence of multiple five-membered rings.

Finally, we sought to further validate our strategy by the preparation of a double helicene which has a sufficient racemization barrier. With the optimized conditions in hands, the synthesis of double azaborahelicenes based on the DHPP skeleton with large steric hindrance, ensuring a stable





Scheme 1 The syntheses of boron complexes **9**, **11** and **13** from DHPP **7**. **8**, **9**: Ar = phenyl, **10**, **11**: Ar = 1-naphthyl, **12**, **13**: Ar = 1-dibenzo[*b,d*]thienyl.

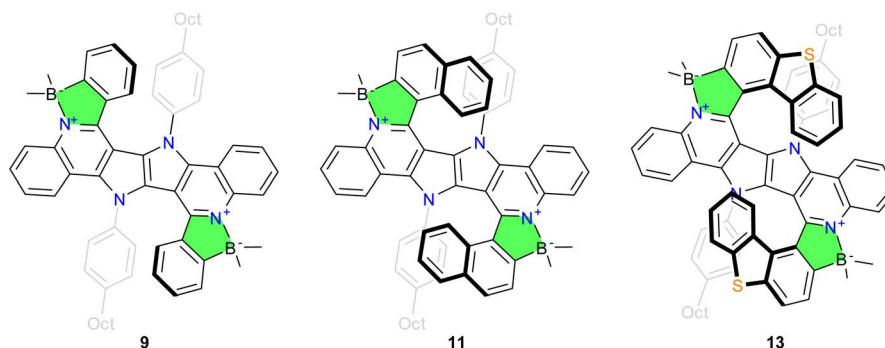


Fig. 2 Chemical structures of the new dyes **9**, **11** and **13**.

configuration, becomes attainable. An aldehyde with an appropriate structure is required for the condensation step, in particular we chose dibenzo[*b,d*]thiophene-1-carbaldehyde, as it can be smoothly obtained in one step from a commercially available substrate. Its condensation with diamino-DHPP, derived from dye **7**, gives **12** in low yield, albeit sufficient for the next step. The final borylation of **12** with  $\text{BBr}_3$ /DBP delivers dye **13**, a double helicene whose configuration is stable at room temperature (Fig. 2). Double helicene **13** was obtained as a racemic mixture, interestingly however that the *meso*-form was not detected. The relatively low yield of double helicene **13** (16%) prompted us to attempt to identify side-products which consists of only traces of the *meso* form among a few unstable substances. Both enantiomers of **13** were successfully isolated using HPLC on a chiral stationary phase with 99.5% enantiomeric excess (ee). Additional details can be found in the ESI.†

## X-ray crystallography

Compound **11** forms large single crystals during purification, which are sufficient for X-ray structural analysis. The experiment confirms the expected structure of **11**, with boron atoms incorporated into the five-membered rings (for another possibility see Fig. S6†). Molecules of **11** crystallize in a centrosymmetric  $P2_1/n$  space group with 4 molecules in the unit cell (Fig. S3†). Out of the two possible diastereoisomers ( $C_i$  and  $C_2$ ) only the chiral forms ( $C_2$ ) are present in the crystal. However, due to the location of the molecule in the general position of the unit cell and the disorder of the octyl substituents, deviations from ideal  $C_2$  symmetry occur. The side chains adopt three alternative positions, as shown in Fig. S4.† The core of the molecule is significantly bent. The angle formed by the outer rings (marked in yellow) is  $37.78(7)^\circ$ . The angles between the planes passing through the rings of the helicene fragments (marked in red and blue) are  $38.14(7)^\circ$  and  $44.22(7)^\circ$ , respectively (Fig. S5†).

Single crystals of **13** was obtained by slow vapor diffusion of diethyl ether into concentrated solution of **13** in dichloromethane. The crystallographic experiment confirms the expected structure of **13** (see Fig. 3). This compound also crystallizes in  $P2_1/n$  space group with 4 molecules in the unit cell (Fig. S8†), similarly to **11**, with a comparable degree of



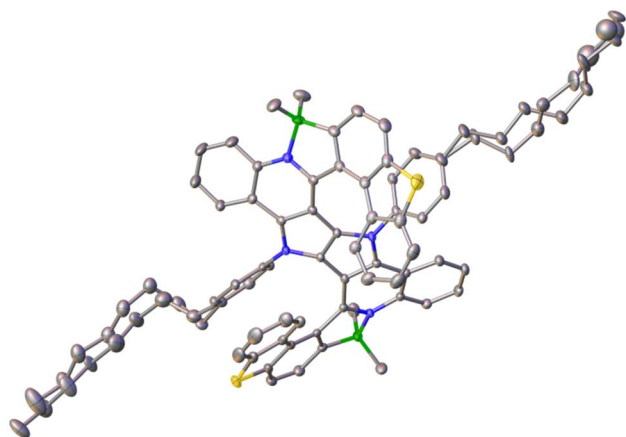


Fig. 3 Structure **13** with anisotropic displacement model at 50% probability level. For clarity, all hydrogen atoms are omitted. CCDC 2430266.

disorder in the octyl chains, which exist in two alternative positions (Fig. S9<sup>†</sup>). The helical part of the molecule is highly curved to the point that the peripheral rings are almost perpendicular to each other.

## Photophysical properties

Having three new helical  $\pi$ -expanded DHPPs **9**, **11** and **13** in hand, we studied their photophysical properties (Fig. 4 and Table 1). The absorption spectra of all the new dyes look similar, with intense absorption bands around 340 nm along with a weaker absorption at 400–450 nm (typical of NB helicenes<sup>43–47</sup>), which is consistent with the computational data (*vide infra*). This correlates well with the structure being a hybrid of double helicenes and a ladder-type  $\pi$ -expanded heterocycle. Additionally, the increase of the chromophore length gives rise to only a moderate bathochromic shift of the absorption maxima. On the other hand,  $\lambda_{\text{abs}}$  values hardly change in different solvents, implying a relatively small change in dipole moment between the two electronic states.

The analysis of the fluorescence spectra shows that the emission of all compounds synthesized is more affected by the solvent polarity. The shape of the emission spectra in non-polar toluene is vibronically-resolved, which is consistent with low inhomogeneous broadening. Increasing the solvent polarity induces a progressive red-shift and broadens the emission band, suggesting a partial charge-transfer character of the emissive state. Dyes **9** and **11** show similar Stokes shift values in each solvent suggesting no specific effect of chromophore expansion on its emission. Lower values of  $\Delta\tilde{\nu}$  for **13** indicate the smallest geometry change upon internal relaxation following photoexcitation within the dyes synthesized.

All the new compounds have fluorescence quantum yields in the range of 0.23 to 0.39, whilst only slightly affected by the solvent polarity. In comparison to known NB helicenes **4–6**, the new dyes exhibit similar spectral profiles, with intense short-wavelength and weak long-wavelength bands, however the  $\Phi_{\text{fl}}$  values are comparable or higher.<sup>43–47</sup> The Stokes shifts of **9**, **11**

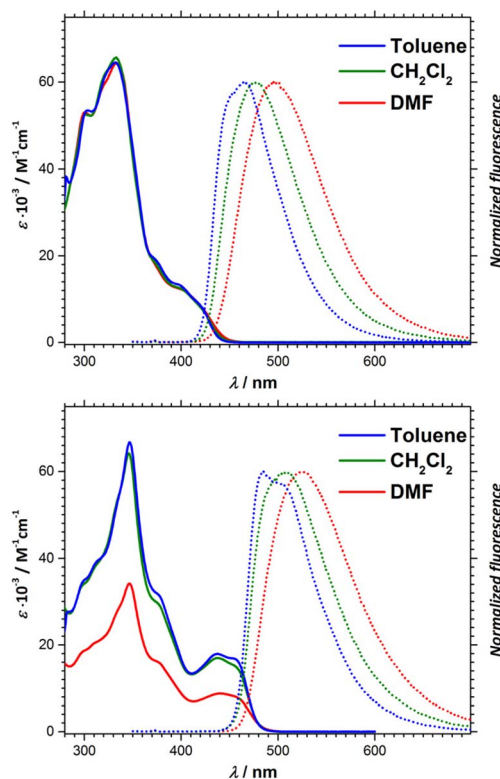


Fig. 4 Absorption (solid line) and emission (dotted line) spectra of compounds **9** (top) and **13** (bottom) in toluene (blue),  $\text{CH}_2\text{Cl}_2$  (green) and DMF (red).

Table 1 Spectroscopic data in toluene (black), dichloromethane (red) and dimethylformamide (blue) for compounds **9**, **11** and **13**<sup>a</sup>

Compound	Solvent	$\lambda_{\text{abs}}$ [nm] ( $\epsilon \cdot 10^{-3}$ [ $\text{cm}^{-1} \text{M}^{-1}$ ])	$\lambda_{\text{em}}$ [nm]	$\Delta\tilde{\nu}$ [ $\text{cm}^{-1}$ ]	$\Phi_{\text{fl}}$
<b>9</b>	Tol	303 (54), 332 (65), 420* (8.5)	465	2300	0.27
	$\text{CH}_2\text{Cl}_2$	301 (53), 333 (66), 420* (8.2)	479	2900	0.23
	DMF	301 (53), 333 (64), 420* (8.5)	496	3600	0.29
<b>11</b>	Tol	343 (61), 420 (19), 440* (16)	489	2300	0.39
	$\text{CH}_2\text{Cl}_2$	342 (63), 420 (19), 440* (15)	499	2700	0.32
	DMF	343 (56), 420 (17), 440* (15)	519	3500	0.34
<b>13</b>	Tol	347 (67), 437 (18), 453* (17)	485	1500	0.34
	$\text{CH}_2\text{Cl}_2$	346 (64), 438 (17), 453* (15)	506	2300	0.30
	DMF	347 (34), 440 (8.8), 453* (8.3)	525	3000	0.38

<sup>a</sup>  $\lambda_{\text{abs}}/\lambda_{\text{em}}$  – absorption/emission wavelength,  $\epsilon$  – molar absorption coefficient,  $\Phi_{\text{fl}}$  – fluorescence quantum yield,  $\Delta\tilde{\nu}$  – Stokes shift. The values of  $\lambda_{\text{abs}}$  marked with an asterisk are estimated, as these maxima are not visible due to overlapping bands.

and **13** are significantly higher than that of **3** and its derivatives, while  $\Phi_{\text{fl}}$  values are approximately 2 times lower, which indicates that the new chromophore is less rigid than that of **3**.<sup>20</sup>

## Chiroptical properties

CD spectra of the enantiomers of dye **13** in DCM (Fig. 5) show multiple peaks, with dissymmetry factors,  $g_{\text{abs}}$ , lower than  $10^{-2}$  (see Fig. S10<sup>†</sup>). The circularly polarized luminescence (CPL) spectra of the enantiomers of **13** in DCM were acquired by



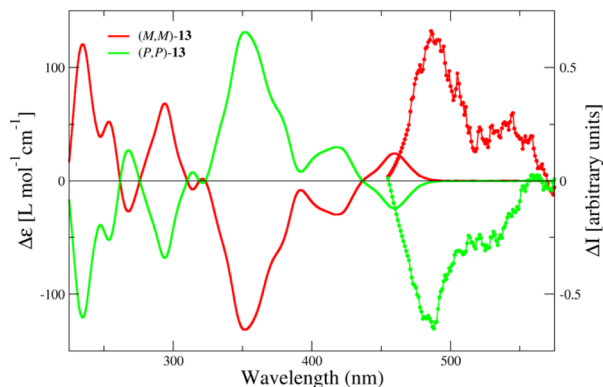


Fig. 5 CD (full lines) and CPL (lines with dots) spectra of the enantiomers of **13** in DCM.

exciting the sample at 410 nm. A horizontal polarizer in excitation was employed to prevent artifacts coming from linearly polarized components of emitted lights.<sup>54</sup> The CPL spectrum has been smoothed using a Savitzky–Golay filter. The shape of the CPL spectrum roughly corresponds to the shape of the emission spectrum in the same solvent (Fig. 4). The dissymmetry factor of CPL,  $|g_{\text{lum}}|$ , is *ca.*  $1.2 \times 10^{-3}$ , consistent with values observed in helicenes with B←N bonds, and indicative of moderate chiral emission activity. Notably, helicene **13** exhibits minimal structural rearrangement in the excited state, as evidenced by the similarity between the  $g_{\text{abs}}$  of the lowest-energy CD band ( $1.7 \times 10^{-3}$ , see Fig. S10†) and  $|g_{\text{lum}}|$ .<sup>55</sup>

To quantify the CPL performance of **13**, the CPL brightness ( $B_{\text{CPL}}$ ) was calculated using the formula:<sup>56</sup>

$$B_{\text{CPL}} = \frac{1}{2} g_{\text{lum}} \Phi_{\text{fl}} \varepsilon$$

where  $\Phi_{\text{fl}}$  is the fluorescence quantum yield and  $\varepsilon$  is the molar absorptivity at a fixed wavelength (usually the absorption maximum). The  $B_{\text{CPL}}$  obtained for **13** in DCM amounts to  $12.1 \text{ M}^{-1} \text{ cm}^{-1}$  (Table 2), classifying the compound as an average CPL emitter.<sup>56</sup>

The chiroptical characterization of **13** was performed in toluene as well (Fig. S10, S11† and Table 2), giving a similar  $|g_{\text{lum}}|$  value but slightly improved  $B_{\text{CPL}}$  ( $15.2 \text{ M}^{-1} \text{ cm}^{-1}$ ) thanks to the higher value of  $\Phi_{\text{fl}}$ .

In order to assign the right absolute configuration to each eluted fraction of **13**, we performed TD-DFT calculations following a procedure detailed in the ESI† and similar to ref. 57 albeit skipping the molecular dynamics simulations sampling because of the high structural rigidity of the chiral chromophoric cores which limits the conformational degrees of

freedom. The comparison of the calculated<sup>58</sup> and experimental CD spectrum shown in Fig. S12† (mainly the sign of the different peaks) allowed us to assign the absolute configuration, in particular the first eluted fraction of **13** corresponds to the (*M,M*) enantiomer.

## Computational studies

We probed the nature of the lowest excited states of dyes **9**, **11**, and **13** in toluene using *ab initio* tools (see the ESI† for computational details). For all three structures, one can envisage both  $C_2$  or  $C_i$  ground-state structures depending on whether the boron-bearing groups are located on the same side of the DHPP plane or not (see Fig. S13 in the ESI† for representation). For all three compounds, theory foresees that the  $C_2$  structures, that are bowl-shaped, are more stable, by 6.9, 6.7, and 7.8  $\text{kcal mol}^{-1}$  (free energy values) than their  $C_i$  counterparts, for dyes **9**, **11**, and **13** respectively. Given that for most “standard” DHPP the two symmetries yield almost the same energies, we attribute this effect to a reduction of the steric stress in the  $C_2$  structures. This is consistent with the crystallographic findings. In the excited state, the structures undergo a slight distortion and become  $C_1$  though their overall shape remains close to the  $C_2$  one. This slight symmetry-breaking is likely at the origin of the solvatofluorochromic effect noticed in the measured emission spectra (*vide supra*).

In the case of dye **9**, the four lowest excited states that could be computed are given in Fig. S14† together with electron density difference (EDD) plots. The lowest excited state of *B* symmetry shows a significant absorption ( $f = 0.372$ ) and corresponds to the shoulder seen in the experimental absorption at *ca.* 400 nm (Fig. 4). The second state is an *A* state with significantly less absorbance. The third transition (*B*) has also a significant probability ( $f = 0.300$ ), whereas the fourth transition (*B*) is very intense ( $f = 1.442$ ) and corresponds to the main band at *ca.* 320 nm in the experimental spectra of Fig. 4. In other words, the combination of these closed four excited states explains the observed absorption spectra.

The electron density different plots corresponding to the lowest excited state of all three compounds can be found in Fig. 6. As can be seen, the lowest excited-states are delocalized over the  $\pi$ -conjugated helical structure with quadrupolar-like charge-transfer, the central DHPP acting as the donor (in blue) and the boron-containing rings as the acceptors (in red). While the topology of the transition remains rather preserved in all three compounds, one notices<sup>58</sup> a slight delocalization on the additional ring (dye **11**) and sulfur atoms (dye **13**), consistent with the observed moderate redshifts. This makes the transitions both more intense and more redshifted, explaining the

Table 2 CPL performance of helicene **13** in toluene and methylene chloride

	$g_{\text{lum}}$ ( <i>M,M</i> )- <b>13</b> / <i>P,P</i> )- <b>13</b>	$\Phi_{\text{fl}}$	$\varepsilon$ @ 350 nm [ $\text{M}^{-1} \text{ cm}^{-1}$ ]	$B_{\text{CPL}}$ [ $\text{M}^{-1} \text{ cm}^{-1}$ ]
Toluene	$+1.32 \times 10^{-3}/-1.24 \times 10^{-3}$	36%	66 000	15.2
DCM	$+1.20 \times 10^{-3}/-1.32 \times 10^{-3}$	29%	66 000	12.1



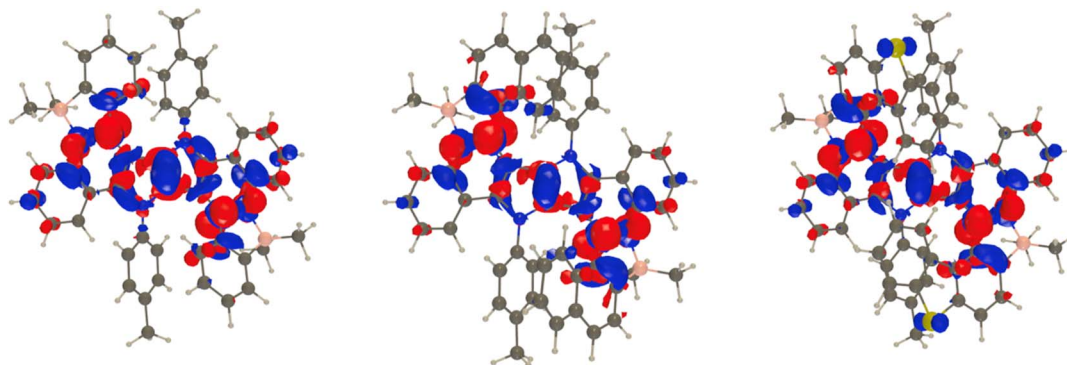


Fig. 6 EDD plots corresponding to the absorption to the lowest state of **9** (left), **11** (center) and **13** (right). The blue and red lobes represent regions of decreased and increased electron density, respectively (threshold: 0.001 au).

clearer band separation between the small first band and the second intense one in **11** and **13** than in **9** found experimentally.

To reach more physically well-grounded comparisons, we have computed the 0–0 energies and performed vibronic calculations. For the former, using a dedicated protocol (see the ESI†), transition energies of 2.64, 2.51, and 2.35 eV are computed for dyes **9**, **11**, and **13**, respectively. These values are in reasonably good agreement (error of *ca.* 0.2 eV) with the absorption-emission crossing point found experimentally, and reproduce the successive redshifts that are obtained experimentally. For the latter, we computed vibrationally-resolved absorption and emission spectra (see Fig. S15 in the ESI†). These computations successfully reproduce the experimental absorption spectra, with all key peaks, especially the shape of 400–440 nm absorption is correctly foreseen. However, the computed molar absorption coefficient of the most intense peak (at *ca.* 300 nm) is approximately  $200\,000\text{ cm}^{-1}\text{ M}^{-1}$  for dyes **9** and **11**, which significantly exceeds their experimental counterparts of *ca.*  $65\,000\text{ cm}^{-1}\text{ M}^{-1}$ . The same relative error is found for the lowest absorption band. In **13**, the computed molar absorption coefficient for the largest peak aligns closely with the experimental value ( $80\,000$  vs.  $67\,000\text{ cm}^{-1}\text{ M}^{-1}$ ) though the computed peaks at *ca.* 400 nm exhibit an excessively large relative intensity in comparison to the experimental value (see Fig. S15†).

## Conclusions

Here we disclose that it is possible to build double helicenes possessing both a 1,4-dihydropyrrolo[3,2-*b*]pyrrole core and nitrogen–boron dative bonds. The efficiency of this convergent approach is underscored by the simplicity of building blocks: two different aromatic aldehydes, a primary aromatic amine, butanedione and a boron source. The method's versatility has been showcased by incorporating such heavily sterically encumbered and demanding moieties as dibenzothiophene-1-yl. Synthesis of N,B-doped nanographenes bearing two [5]helicene scaffolds is very efficient but even in the case of [7]helicene the yields are still acceptable.

The helical, ladder-type molecular architecture translates to the fact that even structures possessing 14 conjugated rings

have absorption maxima located in the UV-blue part of the electromagnetic spectrum. The double helicenes possessing two B←N dative bonds display strong emission in the green region, are sensitive to solvent polarity, and possess moderate circularly polarized luminescence brightness ( $B_{\text{CPL}} = 15\text{ M}^{-1}\text{ cm}^{-1}$ ). Collectively, these results highlight the compatibility of B←N dative bonds with the formation of helical molecular architectures. We anticipate that this chemistry will empower the creation of new materials having BN functionality.

## Data availability

The data supporting this article have been included as part of the ESI.† Deposition number 2415573 contains the supplementary crystallographic data for this paper. The data can be obtained free of charge *via* the joint Cambridge Crystallographic Data Centre (CCDC).

## Author contributions

Conceptualization: W. D. P., D. T. G.; investigation: W. D. P., A. C., F. B., C. N., N. V.; supervision: D. T. G., F. T., M. K. C., D. J.; visualization: W. D. P., A. C., F. B., C. N., N. V.; writing – original draft: W. D. P., F. B., D. J.; F. T., Y. M. P.; D. T. G.; writing – review & editing: W. D. P., F. B., D. J.; C. N., F. T., D. T. G.

## Conflicts of interest

There are no conflicts to declare.

## Acknowledgements

This project has received funding from the European Union's Horizon 2020 Research and Innovation Program under the Marie Skłodowska-Curie grant agreement no. 101007804 and from European Research Council (ARCHIMEDES, 101097337). Views and opinions expressed are, however, those of the authors only and do not necessarily reflect those of the European Union or the European Research Council Executive Agency. Neither the European Union nor the granting authority



can be held responsible for them. The work was also financially supported by the Polish National Science Centre, Poland (OPUS 2020/37/B/ST4/00017) and has benefited from the equipment and framework of the COMP-HUB and COMP-R initiatives, funded by the “Departments of Excellence” program of the Italian Ministry for University and Research (MIUR, 2018-2022 and MUR, 2023-2027). This work was supported by the French Agence Nationale de la Recherche (ANR) under contract ANR-21-CE07-0058-2 (CONDOR). This research used resources of the GLICID Computing Facility (Ligerien Group for Intensive Distributed Computing, 10.60487/glicid, Pays de la Loire, France). The collaboration between the Jacquemin and Gryko group is supported by the Maria Skłodowska-Curie and Pierre Curie Polish-French Science Award of the Académie des Sciences, the FNP and Zygmunt Zaleski foundation. The X-ray structures was determined in the Advanced Crystal Engineering Laboratory (aceLAB) at the Chemistry Department of the University of Warsaw. MKC and AC acknowledges prof. Ilona Turowska-Tyrk for her support.

## Notes and references

- 1 A. Abengózar, P. García-García, M. A. Fernández-Rodríguez, D. Sucunza and J. J. Vaquero, in *Advances in Heterocyclic Chemistry*, Academic Press Inc., 2021, vol. 135, pp. 197–259.
- 2 J. Huang and Y. Li, *Front. Chem.*, 2018, **6**, 341.
- 3 S. K. Mellerup and S. Wang, *Trends Chem.*, 2019, **1**, 77–89.
- 4 S. Nakatsuka, N. Yasuda and T. Hatakeyama, *J. Am. Chem. Soc.*, 2018, **140**, 13562–13565.
- 5 K. Liu, R. A. Lalancette and F. Jäkle, *J. Am. Chem. Soc.*, 2019, **141**, 7453–7462.
- 6 P. B. Pati, E. Jin, Y. Kim, Y. Kim, J. Mun, S. J. Kim, S. J. Kang, W. Choe, G. Lee, H. J. Shin and Y. S. Park, *Angew. Chem., Int. Ed.*, 2020, **59**, 14891–14895.
- 7 J. Hoffmann, B. Geffroy, E. Jaques, M. Hissler and A. Staubitz, *J. Mater. Chem. C*, 2021, **9**, 14720–14729.
- 8 M. Franceschini, M. Crosta, R. R. Ferreira, D. Poletto, N. Demitri, J. P. Zobel, L. González and D. Bonifazi, *J. Am. Chem. Soc.*, 2022, **144**, 21470–21484.
- 9 M. Zhao and Q. Miao, *Angew. Chem., Int. Ed.*, 2021, **60**, 21289–21294.
- 10 M. Fingerle, J. Dingerkus, H. Schubert, K. M. Wurst, M. Scheele and H. F. Bettinger, *Angew. Chem., Int. Ed.*, 2021, **60**, 15798–15802.
- 11 A. Wakamiya, T. Taniguchi and S. Yamaguchi, *Angew. Chem., Int. Ed.*, 2006, **45**, 3170–3173.
- 12 S. Luo, J. Wang, N. Li, X. F. Song, X. Wan, K. Li and C. Yang, *Angew. Chem., Int. Ed.*, 2023, **62**, e202310943.
- 13 T. Sakamaki, T. Nakamuro, K. Yamashita, K. Hirata, R. Shang, E. Nakamura and R. Shang, *Chem. Mater.*, 2021, **33**, 5337–5344.
- 14 K. Liu, R. A. Lalancette and F. Jäkle, *J. Am. Chem. Soc.*, 2017, **139**, 18170–18173.
- 15 M. Vanga, R. A. Lalancette and F. Jäkle, *Chem.–Eur. J.*, 2019, **25**, 10133–10140.
- 16 M. Vanga, A. Sahoo, R. A. Lalancette and F. Jäkle, *Angew. Chem., Int. Ed.*, 2022, **61**, e202113075.
- 17 K. Liu, Z. Jiang, R. A. Lalancette, X. Tang and F. Jäkle, *J. Am. Chem. Soc.*, 2022, **144**, 18908–18917.
- 18 R. Campos-González, P. Vázquez-Domínguez, P. Remón, F. Nájera, D. Collado, E. Pérez-Inestrosa, F. Boscá, A. Ros and U. Pischel, *Org. Chem. Front.*, 2022, **9**, 4250–4259.
- 19 H. Lu, T. Nakamuro, K. Yamashita, H. Yanagisawa, O. Nureki, M. Kikkawa, H. Gao, J. Tian, R. Shang and E. Nakamura, *J. Am. Chem. Soc.*, 2020, **142**, 18990–18996.
- 20 M. Tasiór, P. Kowalczyk, M. Przybył, M. Czichy, P. Janasik, M. H. E. Bousquet, M. Łapkowski, M. Rammo, A. Rebane, D. Jacquemin and D. T. Gryko, *Chem. Sci.*, 2021, **12**, 15935–15946.
- 21 Y. Shen and C. F. Chen, *Chem. Rev.*, 2012, **112**, 1463–1535.
- 22 Y. Zhang, S. Yu, B. Han, Y. Zhou, X. Zhang, X. Gao and Z. Tang, *Matter*, 2022, **5**, 837–875.
- 23 T. Mori, *Chem. Rev.*, 2021, **121**, 2373–2412.
- 24 J. Han, S. Guo, H. Lu, S. Liu, Q. Zhao and W. Huang, *Adv. Opt. Mater.*, 2018, **6**, 1–32.
- 25 J. Full, M. J. Wildervanck, C. Dillmann, S. P. Panchal, D. Volland, F. Full, K. Meerholz and A. Nowak-Król, *Chem.–Eur. J.*, 2023, **29**, e202302808.
- 26 P. Stachelek, L. MacKenzie, D. Parker and R. Pal, *Nat. Commun.*, 2022, **13**, 553.
- 27 C. Li, Y. Yang and Q. Miao, *Chem.–Asian J.*, 2018, **13**, 884–894.
- 28 W. W. Yang and J. J. Shen, *Chem.–Eur. J.*, 2022, **28**, e202202069.
- 29 X. Y. Wang, X. C. Wang, A. Narita, M. Wagner, X. Y. Cao, X. Feng and K. Müllen, *J. Am. Chem. Soc.*, 2016, **138**, 12783–12786.
- 30 F. Aribot, A. Merle, P. Dechambenoit, H. Bock, A. Artigas, N. Vanthuyne, Y. Carissan, D. Hagebaum-Reignier, Y. Coquerel and F. Durola, *Angew. Chem., Int. Ed.*, 2023, **62**, e202304058.
- 31 A. Artigas, F. Rigoulet, M. Giorgi, D. Hagebaum-Reignier, Y. Carissan and Y. Coquerel, *J. Am. Chem. Soc.*, 2023, **145**, 15084–15087.
- 32 Y. F. Wu, S. W. Ying, S. Di Liao, L. Zhang, J. J. Du, B. W. Chen, H. R. Tian, F. F. Xie, H. Xu, S. L. Deng, Q. Zhang, S. Y. Xie and L. S. Zheng, *Angew. Chem., Int. Ed.*, 2022, **61**, e202204334.
- 33 M. Akiyama and K. Nozaki, *Angew. Chem., Int. Ed.*, 2017, **56**, 2040–2044.
- 34 M. Schnitzlein, K. Shoyama and F. Würthner, *Chem. Sci.*, 2024, **15**, 2984–2989.
- 35 F. Saal, F. Zhang, M. Holzapfel, M. Stolte, E. Michail, M. Moos, A. Schmiedel, A. M. Krause, C. Lambert, F. Würthner and P. Ravat, *J. Am. Chem. Soc.*, 2020, **142**, 21298–21303.
- 36 C. Dusold, D. I. Sharapa, F. Hampel and A. Hirsch, *Chem.–Eur. J.*, 2021, **27**, 2332–2341.
- 37 S. S. Warthegau, A. E. Hillers-Bendtsen, S. K. Pedersen, C. Rindom, C. Bræstrup, J. S. Jensen, O. Hammerich, M. S. Thomsen, F. S. Kamounah, P. Norman, K. V. Mikkelsen, T. Brock-Nannestad and M. Pittelkow, *Chem.–Eur. J.*, 2023, **29**, 1–6.
- 38 D. Tan, J. Dong, T. Ma, Q. Feng, S. Wang and D. T. Yang, *Angew. Chem., Int. Ed.*, 2023, **62**, e202304711.



- 39 T. Katayama, S. Nakatsuka, H. Hirai, N. Yasuda, J. Kumar, T. Kawai and T. Hatakeyama, *J. Am. Chem. Soc.*, 2016, **138**, 5210–5213.
- 40 A. Nowak-Król, P. T. Geppert and K. R. Naveen, *Chem. Sci.*, 2024, **15**, 7408–7440.
- 41 Y. Appiarius, S. Míguez-Lago, P. Puylaert, N. Wolf, S. Kumar, M. Molkenhain, D. Miguel, T. Neudecker, M. Juriček, A. G. Campaña and A. Staubitz, *Chem. Sci.*, 2023, **15**, 466–476.
- 42 K. Yuan, D. Volland, S. Kirschner, M. Uzelac, G. S. Nichol, A. Nowak-Król and M. J. Ingleson, *Chem. Sci.*, 2022, **13**, 1136–1145.
- 43 J. Full, S. P. Panchal, J. Götz, A. M. Krause and A. Nowak-Król, *Angew. Chem., Int. Ed.*, 2021, **60**, 4350–4357.
- 44 F. Full, Q. Wölflick, K. Radacki, H. Braunschweig and A. Nowak-Król, *Chem.–Eur. J.*, 2022, **28**, e202202280.
- 45 F. Full, M. J. Wildervanck, D. Volland and A. Nowak-Król, *Synlett*, 2023, **34**, 477–482.
- 46 D. Volland, J. Niedens, P. T. Geppert, M. J. Wildervanck, F. Full and A. Nowak-Król, *Angew. Chem., Int. Ed.*, 2023, **62**, e202304291.
- 47 F. Full, A. Artigas, K. Wiegand, D. Volland, K. Szkodzinska, Y. Coquerel and A. Nowak-Król, *J. Am. Chem. Soc.*, 2024, **146**, 29245–29254.
- 48 A. Janiga, E. Glodkowska-Mrowka, T. Stokłosa and D. T. Gryko, *Asian J. Org. Chem.*, 2013, **2**, 411–415.
- 49 M. Krzeszewski, D. Gryko and D. T. Gryko, *Acc. Chem. Res.*, 2017, **50**, 2334–2345.
- 50 G. Sanil, B. Koszarna, Y. M. Poronik, O. Vakuliuk, B. Szymański, D. Kusy and D. T. Gryko, in *Advances in Heterocyclic Chemistry*, Academic Press Inc., 2022, vol. 138, pp. 335–409.
- 51 M. Tasiór, M. Chotkowski and D. T. Gryko, *Org. Lett.*, 2015, **17**, 6106–6109.
- 52 N. Ishida, T. Moriya, T. Goya and M. Murakami, *J. Org. Chem.*, 2010, **75**, 8709–8712.
- 53 D. L. Crossley, I. A. Cade, E. R. Clark, A. Escande, M. J. Humphries, S. M. King, I. Vitorica-Yrezabal, M. J. Ingleson and M. L. Turner, *Chem. Sci.*, 2015, **6**, 5144–5151.
- 54 G. Longhi, E. Castiglioni, J. Koshoubu, G. Mazzeo and S. Abbate, *Chirality*, 2016, **28**, 696–707.
- 55 J. L. Greenfield, J. Wade, J. R. Brandt, X. Shi, T. J. Penfold and M. J. Fuchter, *Chem. Sci.*, 2021, **12**, 8589–8602.
- 56 L. Arrico, L. Di Bari and F. Zinna, *Chem.–Eur. J.*, 2021, **27**, 2920–2934.
- 57 G. Pescitelli and T. Bruhn, *Chirality*, 2016, **28**, 466–474.
- 58 M. J. Frisch, G. W. Trucks, H. B. Schlegel, G. E. Scuseria, M. A. Robb, J. R. Cheeseman, G. Scalmani, V. Barone, G. A. Petersson, H. Nakatsuji, X. Li, M. Caricato, A. V. Marenich, J. Bloino, B. G. Janesko, R. Gomperts, B. Mennucci, H. P. Hratchian, J. V. Ortiz, A. F. Izmaylov, J. L. Sonnenberg, D. Williams-Young, F. Ding, F. Lipparini, F. Egidi, J. Goings, B. Peng, A. Petrone, T. Henderson, D. Ranasinghe, V. G. Zakrzewski, J. Gao, N. Rega, G. Zheng, W. Liang, M. Hada, M. Ehara, K. Toyota, R. Fukuda, J. Hasegawa, M. Ishida, T. Nakajima, Y. Honda, O. Kitao, H. Nakai, T. Vreven, K. Throssell, J. A. Montgomery, J. E. Peralta Jr, F. Ogliaro, M. J. Bearpark, J. J. Heyd, E. N. Brothers, K. N. Kudin, V. N. Staroverov, T. A. Keith, R. Kobayashi, J. Normand, K. Raghavachari, A. P. Rendell, J. C. Burant, S. S. Iyengar, J. Tomasi, M. Cossi, J. M. Millam, M. Klene, C. Adamo, R. Cammi, J. W. Ochterski, R. L. Martin, K. Morokuma, O. Farkas, J. B. Foresman and D. J. Fox, *Gaussian 16 (Revision A.03)*, Gaussian Inc., Wallingford CT, 2016.

